Available online at www.sciencedirect.com

ScienceDirect

Ceramics International 40 (2014) 4471–4477

CERAMICS INTERNATIONAL

www.elsevier.com/locate/ceramint

Electrical properties of Ag-doped ZnO nano-plates synthesized via wet chemical precipitation method

Reza Zamiri[a,*], B.K. Singh[b], Dibakar Dutta[c], Avito Reblo[a], J.M.F. Ferreira[a]

[a]Department of Materials Engineering and Ceramic, CICECO, University of Aveiro, Campus Santiago, 3810-193 Aveiro, Portugal
[b]TEMA-NRD, Mechanical Engineering Department and Aveiro Institute of Nanotechnology (AIN), University of Aveiro, 3810-193 Aveiro, Portugal
[c]Department of Physics, University of Aveiro, Campus Santiago, 3810-193 Aveiro, Portugal

Received 3 August 2013; received in revised form 27 August 2013; accepted 28 August 2013
Available online 7 September 2013

Abstract

Ag-doped and pure zinc oxide (ZnO) nano-plates were successfully synthesized via low cost wet precipitation method. The crystalline phases and the morphological features of the synthesized samples were assessed by X-ray diffraction (XRD) and scanning electron microscopy. These techniques coupled with Energy-dispersive X-ray spectroscopy (EDS) measurements confirmed the incorporation of Ag element into the ZnO matrix. The dielectric loss and ac conductivity were studied as a function of frequency and composition. A detailed analysis of the dielectric loss and ac conductivity as a function of composition were done in a wide frequency range at room temperature. In addition, the charge transport mechanism through the grain and grain boundary regions were investigated using impedance spectroscopy analysis.

Keywords: C. Dielectric properties; Impedance spectroscopy; ZnO nanoplate

1. Introduction

ZnO is a wide band gap semiconductor ($E_g = 3.3$ eV) with large free exciton binding energy (60 meV), which makes it a good candidate for semiconductor device applications such as piezoelectric transducers, short wavelength optical devices, transparent conductive films, solar cell windows, optical waveguides and varistors [1–5]. On the other hand, the nanostructures of ZnO have attracted much attention due to their unique properties [6,7]. So far, ZnO nanostructures with different shapes have been widely fabricated because of their easy formation and their potential applications in many important areas [8–12].

A unique feature of nanostructures is the large surface to volume ratio available in these systems. They consists of grains, grain boundaries and grain interfaces which play important roles in the determination of the electrical properties [13,14]. The grain boundaries having high density of defects like dangling bonds, vacancies, micropores etc., can control the transport properties of the material in a decisive manner. Dielectric behavior is one of the most important properties of material, which markedly depends on the preparation conditions. Furthermore, the high excitonic binding energy of ZnO depends on the dielectric constant of the material and material with high dielectric constant has numerous applications in microelectronics. Many researchers have investigated the dielectric properties of ZnO nanostructures in the near past [13,15,16].

A very elegant experimental method to study transport in grain interior (bulk) and at interfaces is impedance spectroscopy, which has emerged over the past several years as a powerful technique for the electrical characterization. In this paper, we have successfully investigated the electrical properties of pure and Ag-doped ZnO nano-plate synthesized by precipitation technique. Furthermore, the various phenomena owing to its enhanced electrical properties have been discussed and correlated with various experimental results viz. X-ray diffraction, dielectric and impedance spectroscopy.

2. Experimental procedure

2 mol% Ag-doped ZnO nanoplates were prepared by wet chemical precipitation method. High purity $Zn(NO_3)_2 \cdot 6H_2O$ (Aldrich, Germany) and $Ag(NO_3)$ (Aldrich, Germany), were

*Corresponding author. Tel.: +351 60173399431; fax: +351 603 89454454.
E-mail addresses: rezaz@ua.pt, Zamiri.r@gmail.com (R. Zamiri).

0272-8842/$ - see front matter © 2013 Elsevier Ltd and Techna Group S.r.l. All rights reserved.
http://dx.doi.org/10.1016/j.ceramint.2013.08.120

chosen as the source material for zinc and silver, respectively, and dissolved in de-ionized water. The obtained precursor solutions were dropped into100 mL of NaOH (MERK) (0.1 M) solution to obtain pure and Ag-doped ZnO precipitates. The alkalinity of all precipitated suspensions was kept constant at pH ~13. Finally, the precipitated particles were separated by centrifugation and washed several times with distilled water for the complete removal of sodium ions. The washed precipitates were then dried at 80 °C for 24 h followed by further heat treatment at 275 °C for 2 h to obtain the powders. The chemical reactions that occurred during preparation were as follows:

$$Zn(NO_3)_2 + 2\,NaOH \rightarrow Zn(OH)_2 + 2NaNO_3$$

$$Zn(OH)_2 \rightarrow ZnO + H_2O$$

$$2AgNO_3 + 2\,NaOH \rightarrow 2AgOH + 2NaNO_3$$

$$2AgOH \rightarrow Ag_2O + H_2O$$

The structure and morphology of the samples were studied by X-ray diffractometry (Shimadzu XRD-6000, Tokyo, Japan) and scanning electron microscopy (SEM). The composition of Ag-doped sample was studied by EDS. The optical properties of the samples were carried out by Raman spectrometry. For the measurement of electrical properties, cylindrical disks with 10 mm diameter and ~2 mm thickness were prepared by dry pressing under 1 t pressure, and top conductive electrodes were deposited on both sides using silver paste. Dielectric constant and loss were measured at room temperature in wide frequency range from 100 Hz to 1 MHz, using an impedance analyzer (4294A, Agilent, USA).

3. Results and discussions

Fig. 1 shows the XRD patterns of pure and Ag-doped ZnO nano-plates. Pure ZnO pattern shows well crystalline hexagonal wurtzite phase (JCPDS no. 36-1451), whereas, Ag-doped ZnO exhibits the same ZnO wurtzite phase and some additional peaks corresponding to fcc metallic Ag phase (JCPDS no. 04-0783). Appearance of Ag peaks in the diffraction pattern clearly indicates the formation of crystalline silver clusters in the nano-plates. It is worth mentioning that Ag^+ ions in ZnO lattice behave similar to other monovalent dopant ions like Na^+ and K^+, which have the ability to occupy both the lattice and interstitial sites [17]. However only a limited incorporation of Ag^+ ions into the ZnO lattice through substitution of Zn^{2+} ions is expected due to a large difference in their ionic radii viz. Ag^+ (1.22 Å) as compared to Zn^{2+} (0.74 Å). Further, Reitveld analyses were made to quantitatively confirm the amount of Ag present as a cluster with ZnO in the doped sample, whose results are tabulated in Table 1. The results suggested the incorporation of only a 0.52% of Ag ions in the ZnO matrix and presence of 1.48% of Ag ions as a cluster in the sample.

Fig. 2 shows the SEM images of pure and Ag-doped ZnO nano-structures. Vertically aligned nanoplates like structures with an average thickness of 100 nm and width in the range 300–500 nm

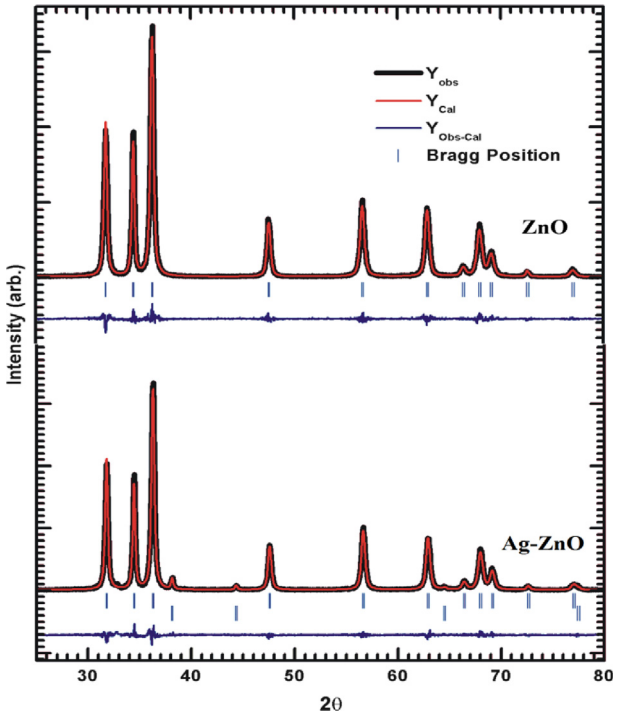

Fig. 1. X-ray diffraction patterns of pure and Ag-doped ZnO nanoplates.

is evident from the SEM micro-photograph. The corresponding selected area electron diffraction patterns showed high crystal quality of the samples. Fig. 3 shows the EDS spectra for Ag doped samples. From EDS spectra we observed the presence of Ag in Ag-doped ZnO powder.

Fig. 4 shows the Raman spectra for pure and Ag-doped ZnO nano-plates, in the range from 200 to 800 cm^{-1}. Five different peaks at 328, 378, 437, 580 and 658 cm^{-1} were observed in case of pure ZnO sample, which correspond to $3E_{2H}$–$3E_{2L}$, A_1(TO), E_{2H}, A_1(LO) and $2(E_{2H}$–$2E_{2L})$ respectively. However, in case of Ag-doped ZnO nano-plates sample, A_1(LO) peak broadened and shifts toward higher energy. Such a broadening and shift in this phonon mode can be attributed to the scattering contributions of A_1(LO) branch outside the Brillouin zone center. The A_1(LO) phonon mode is commonly attributed to the zinc interstitials, oxygen vacancies or defect complexes containing zinc interstitial and oxygen vacancy in ZnO [18]. In addition, the presence of a broad peak at about 487 cm^{-1} can be assigned as the interfacial surface phonon mode as reported elsewhere [19]. The peak appearing at ~690 cm^{-1} has also been reported for Co-doped ZnO [20] and the origin is not yet clear. The intensity of E_{2H} mode has been found to decrease discontinuously with Ag-doping, which could be due to the breakdown of translational crystal symmetry by the incorporated defects and impurities.

Dielectric properties of the materials are characterized by the complex permittivity given by $\varepsilon^* = \varepsilon_1 + j\varepsilon_2$ (where ε_1 and ε_2 are real part and imaginary parts of complex permittivity). Under an application of electric field, the stored energy in any dielectric material corresponds to real parts of dielectric constant, whereas dissipated energy corresponds to imaginary parts of dielectric constant. Fig. 5a and b shows the variation of real (ε_1) and imaginary (ε_2) parts of dielectric constant with frequency.

Table 1
Reitveld refinement results for pure and Ag doped samples.

Sample	System	Space group	*a*	*b*	*c*	*V*	*c/a*	R_b	R_p	R_{wp}	χ^2	Fraction (%)
Pure	Hexagonal	P63mc	3.2506(2)		5.2063(3)	47.64	1.6017	1.15	7.27	11.3	3.948	100
Doped	Hexagonal	P63mc	3.2500(2)		5.2064(3)	47.62	1.602	1.1	7.56	11.8	3.422	98.52
	Cubic (Ag)	Fm3m	4.0865(4)			68.24	1	5.39	7.56	11.8	3.422	1.48

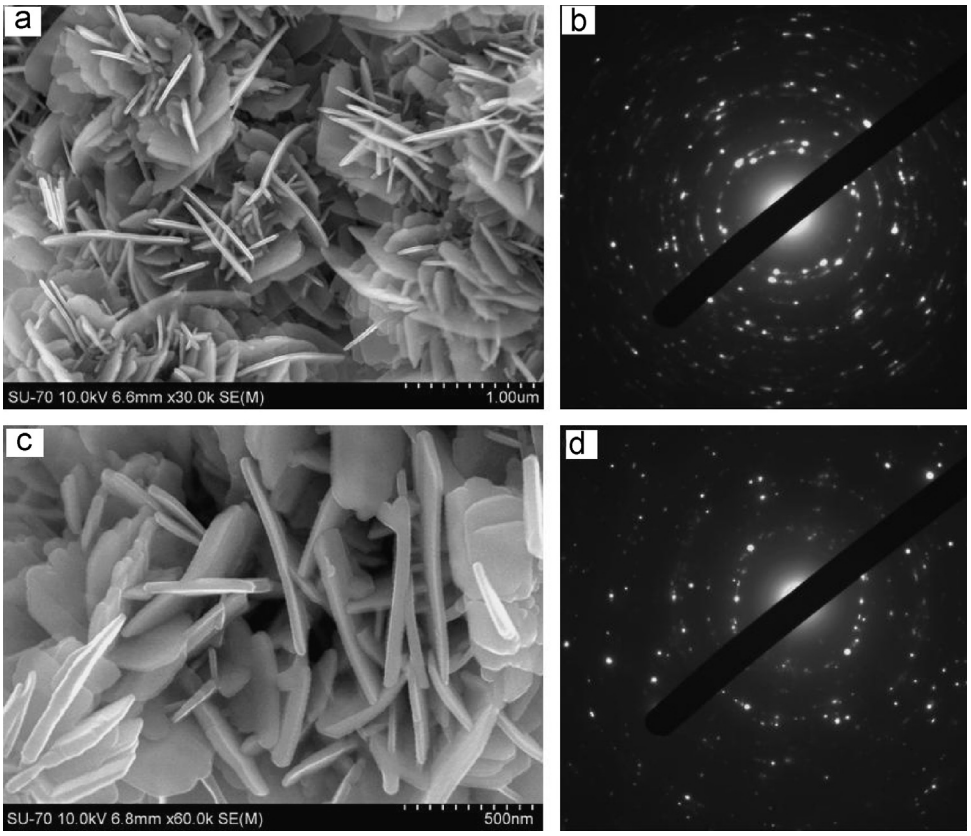

Fig. 2. SEM micrographs and corresponding SAED patterns of pure (a and b) and Ag-doped (c and d) ZnO nano-plates.

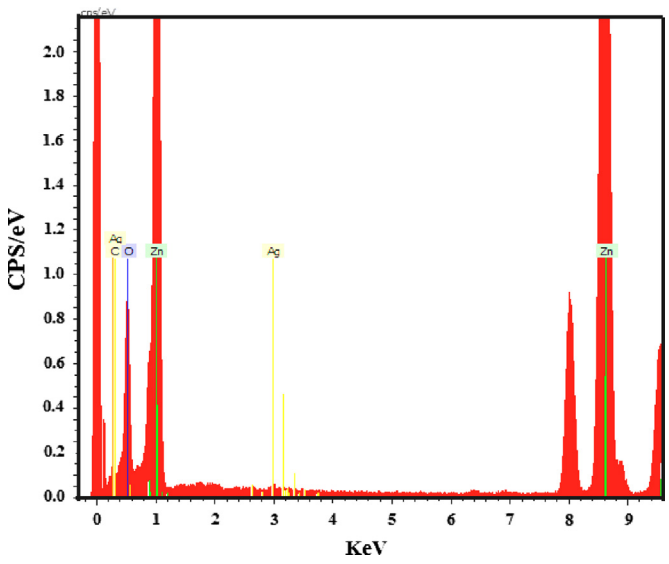

Fig. 3. EDS spectrum of Ag-doped ZnO nano-plates.

A decreases in the real dielectric constant with increasing frequency for pure and doped samples are observed. Furthermore, beyond a specific frequency, frequency independent responses of dielectric constant are seen.

However, two different behaviors were observed for pure and doped samples. For frequencies below 10 kHz the value of dielectric constant was found to be higher for pure ZnO, however, above this frequency the situation reversed. It is well-known that the large values of dielectric constant and dielectric loss at frequencies below 1 kHz are due to the existence of space charge polarization in the nano-structure. Above this frequency the orientational polarization is the dominant mechanism [7,21,22]. This suggests that the space charge polarization is stronger in the case of pure ZnO nano-plates whereas, orientational polarization is stronger for Ag-doped ZnO nano-plates.

The ZnO nanostructures exhibit space charge polarization due to their structural inhomogeneities. The nanostrucutres contain a number of surface defects such as dangling bonds, vacancies and micropores at the grain boundaries due to their large surface-to-

volume ratio. These surface defects cause a change of positive and negative space charge distributions at the interfaces. When an external electric field is applied these space charges move under the field and are trapped by defects at the interfaces, forming dipoles. At low frequencies, hopping electrons are trapped by these structural inhomogeneities which lead to a dominant space charge polarization at low frequencies. On the other hand, rotational displacement of dipoles in the nanostructures at higher frequencies results in this orientational polarization. The possible source of orientational polarization is the existence oxygen vacancies and zinc interstitials in the nano-sized ZnO. There is a tendency of the occupied cations to be associated with the positive ion vacancies, so that the associated pairs have dipole moments. When an external field is applied, the Zn^{2+} ions and the O^{2-} vacancies in the neighborhood can exchange the positions by a single jump and try to align along the direction of field. The presence of Ag dopant increases the amount of oxygen vacancies and zinc interstitials in crystal, which lead to an increase of dipole moment and, in turn, to orientational polarization.

At higher frequencies, the space charges cannot follow the change of the field and hence do not produce space charge polarization. The dipoles are also unable to follow rapidly with varying electric field. Damping of these dipoles accounts for the reduction of dielectric constant at higher frequencies.

Fig. 6 shows the variations of dielectric loss with frequency for both pure and Ag-doped ZnO nanostructures. The following equation can be used to obtain loss tangent:

$$\tan\ \delta = \frac{\varepsilon_2}{\varepsilon_1} \quad (1)$$

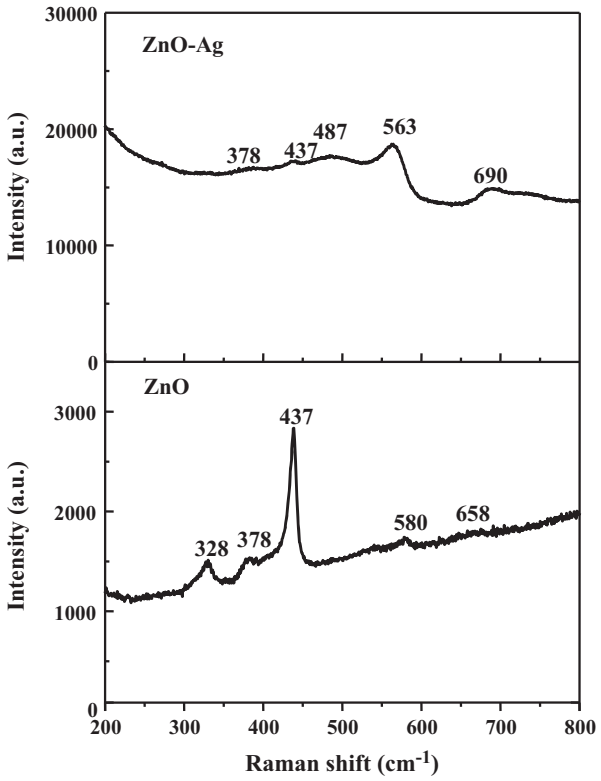

Fig. 4. Raman spectra of pure and Ag-doped ZnO nano-plates.

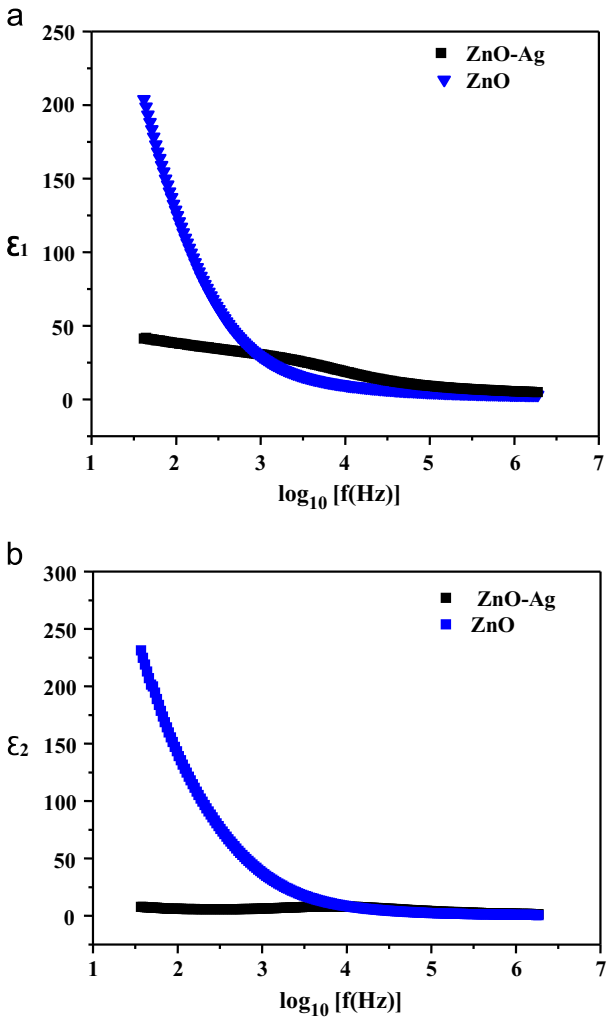

Fig. 5. Variation of real and imaginary part of dielectric constant with frequency for pure and Ag-doped ZnO nanoplates.

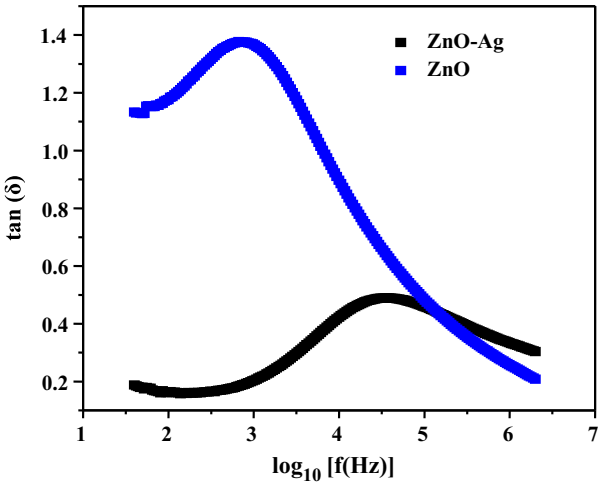

Fig. 6. Variation of dielectric loss with frequency for pure and Ag-doped ZnO nano-plates.

Both the spectrums display one peak at certain frequency which is shifted to higher frequency with Ag doping. This peak represents the relaxation process and occurs when frequency of

the applied ac field is approximately equal to the frequency of hopping of the localized charge carrier [23]. The maximum loss tangent can be observed in following condition [24]:

$$\omega_0 \tau = 1 \tag{2}$$

where τ is relaxation time and $\omega_0 = 2\pi f$ is the angular frequency. On the other hand, hoping probability per unit time p is related to relaxation time through the following equation:

$$\tau = \frac{1}{2p} \tag{3}$$

The calculated relaxation times of pure and Ag-doped ZnO nanostructures are 25×10^{-5} and 39×10^{-7} respectively. This decrease in the relaxation time with Ag-doping signifies an increase in the hopping probability. This is consistent with the results obtained for the frequency dependence curve of real part of dielectric constant. Moreover, from Fig. 6 it can be seen that the loss is decreased after Ag-doping and gradually decreases in the higher frequency regime.

The ac conductivity was found to increase with the frequency for both of the samples. In general, total conductivity can be expressed by the summation of the band and the hopping parts:

$$\sigma_{tot} = \sigma_0(T) + \sigma(\omega,\ T)$$

The first term in above equation is dc conductivity due to the band conduction, which is frequency independent whereas, the second term is the pure ac conductivity due to migration of electric charge carriers between the metal ions. It has been reported that the ac conductivity gradually increases with the increase in frequency of applied ac field because the increase in frequency enhances the migration of electron [16,25]. Fig. 7 also reveals the decrease of conductivity with Ag doping in ZnO matrix. It can be explained considering that the presence of Ag ions introduce defects such as zinc interstitials and oxygen vacancies in the ZnO crystal lattice. These defects tend to segregate at the grain boundaries due to diffusion process and therefore facilitate the formation of grain boundary defect barrier leading to blockage to the flow of charge carriers. This in turn decreases the conductivity of the system on Ag-doping.

Impedance spectroscopy has been widely used to study the charge transport behavior in nano-crystalline materials. This analysis provides a correlation between the electrical and structural properties of the material. The electrical phenomenon due to bulk material, grain boundary and interfacial phenomenon appears in the form of arc of a semicircle, when components of impedance are plotted in a complex argand planes (Nyquist plots). Fig. 8 shows impedance Nyquist plots of pure and Ag doped ZnO nanoplate samples (plotting the imaginary parts of z'' versus the real part z' at room temperature). Generally, the grains are effective in high frequency region while the grain boundaries are effective in low frequency region [26]. Single circular arc type behavior was observed in the Nyquist plot for both pure and Ag-doped ZnO samples, which suggests the predominance of grain boundary resistance over the grain resistances.

The real and imaginary parts of total impedance are defined by following equations:

$$Z^* = Z' - jZ'' \tag{4}$$

$$Z' = R + \frac{R_g}{1+(\omega R_g C_g)^2} + \frac{R_{gb}}{1+(\omega R_{gb} C_{gb})^2} \tag{5}$$

$$Z'' = R_g\left[\frac{\omega R_g C_g}{1+(\omega R_g C_g)^2}\right] + R_{gb}\left[\frac{\omega R_{gb} C_{gb}}{1+(\omega R_{gb} C_{gb})^2}\right] \tag{6}$$

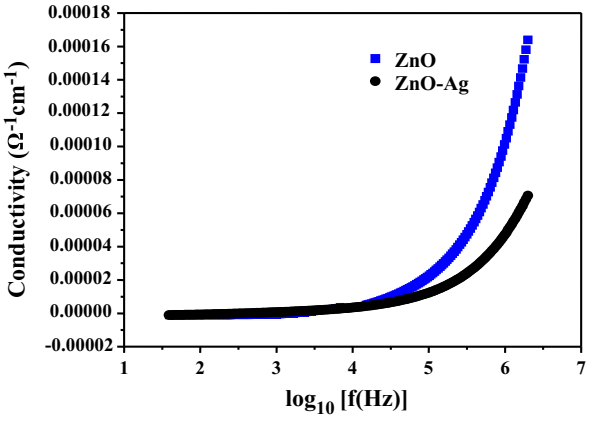

Fig. 7. Variation of ac conductivity with frequency for pure and Ag doped ZnO nanoplates at room temperature.

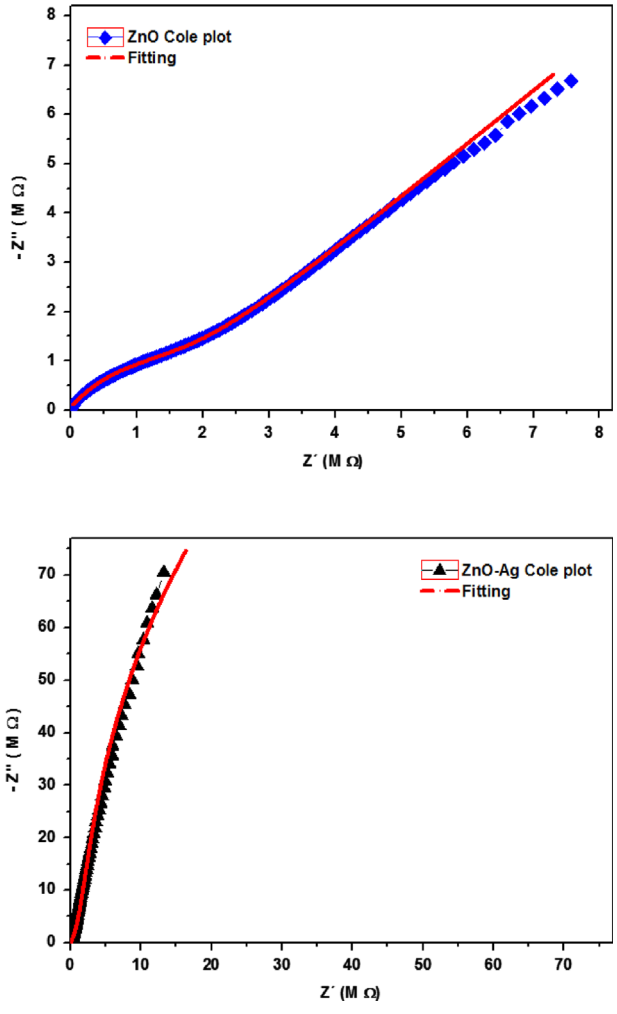

Fig. 8. Nyquist plots for pure and Ag-doped ZnO nano-plates.

where R_g, R_{gb}, C_g and C_{gb} are grain and grain boundary resistance as well as grain and grain boundary capacitance. The capacitance and relaxation times of grain and grain boundary (τ_g, τ_{gb}) are related by the following equations:

$$C_g = \frac{1}{R_g \omega_g} \tag{7}$$

$$C_{gb} = \frac{1}{R_{gb} \omega_{gb}} \tag{8}$$

$$\tau_g = R_g C_g \tag{9}$$

$$\tau_{gb} = R_{gb} C_{gb} \tag{10}$$

These parameters are obtained by analyzing the impedance data on nonlinear least square (NLLS) fit method and listed in Table 2.

According to Table 2, the grain boundary resistance R_{gb} increases while the capacitance C_{gb} decreases after doping. This might be due to introduction of Ag ion in ZnO matrix, which increases the defect ions concentration tending to segregation at grain boundaries forming grain boundary defect barriers [27]. As dopant increases, barrier height increase which results in decrease of C_{bg} as it is inversely proportional to barrier height [28] as follows:

$$C_{gb} = \frac{n^{1/2}}{\varnothing_B{}^{1/2}} \tag{10}$$

here C_{gb} is the grain boundary capacitance, n is the concentration of charge carriers and $\varnothing_B$ is the barrier height. Due to the presence of large number of grain boundaries in both the samples, grain boundary contribution becomes dominant and grain contribution is not resolved. Due to this fact, the single circular arc is being observed in Cole–Cole plots. Moreover, it can be seen from Fig. 8 that total impedance increases with doping content which is in agreement with conductivity analysis.

The electric modulus M^* is defined by the following equation:

$$M^* = \frac{1}{\varepsilon^*} = \frac{1}{\varepsilon' - j\varepsilon''} = \frac{\varepsilon'}{\varepsilon'^2 + \varepsilon''^2} + j\frac{\varepsilon'}{\varepsilon'^2 + \varepsilon''^2} = M'(\omega) + jM''(\omega) \tag{11}$$

$$= M_\infty \left[1 - \int_0^\infty e^{-j\omega t} \left(\frac{d\varnothing(t)}{dt}\right) dt\right] \tag{12}$$

Table 2
Impedance parameters for pure and Ag doped ZnO nano-plates.

Sample	R_{gb} (Ω)	C_{gb} (nF)	τ_{gb} (s)
ZnO	1.2E6	3.24E−10	3.88E−4
ZnO–Ag	2.34E8	4.34E−11	10.15E−3

where M' and M'' are real and imaginary part of electric modulus and $\varnothing(t)$ gives the time evolution of the electric field within the dielectric. The electric modulus is a useful function to eliminate electrode effects [29]. Fig. 9 shows the frequency variation of the real part M' of the electric modulus for pure and Ag-doped samples. The values of M' at lower frequency for both of the samples were found to be extremely small, demonstrating that electrode polarization can be neglected and does not contribute to the large dielectric values. The frequency dependence of $M'(\omega)$ and $M''(\omega)$ for pure and Ag-doped ZnO nano-plates are shown in Fig. 9 $M'(\omega)$ values are observed to tend towards M_∞ (the asymptotic value of $M'(\omega)$) at higher frequencies, whereas $M''(\omega)$ exhibits a maximum at certain frequency. As it can be seen from Fig. 9b, after Ag-doping the position of the peak shifted to higher frequencies. The frequency region below peak maximum ($M''(\omega)$) determines the range in which charge carriers are mobile on long distances. At frequency above peak maximum, the carriers are confined to potential wells, being mobile on short distances. The maximum peak frequency ω_m (corresponding to M_m'') gives the most probable relaxation time τ_m from the condition $\tau_m \omega_m = 1$.

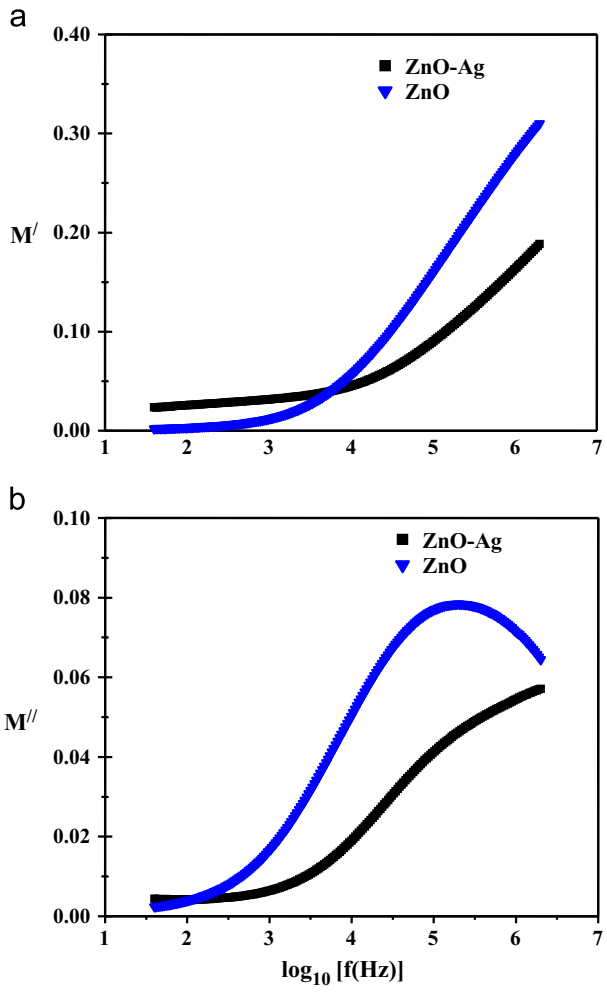

Fig. 9. Variation of electric modulus with frequency for pure and Ag-doped ZnO nano-plates.

4. Conclusions

Pure and Ag-doped ZnO nano-plates have been successfully synthesized by the precipitation method as confirmed by XRD analysis and SEM morphological observations. Raman spectroscopy showed that ZnO lattice was disturbed by the Ag-doping with Ag atoms accumulating at the interstitial sites, breaking down the translational symmetry. The dielectric relaxation mechanism was due to space charge polarization at low frequencies and orientational polarization at high frequencies. The space charge polarization was found to be stronger in the case of pure ZnO nano-plates whereas, orientational polarization was found to be stronger for Ag-doped ZnO nano-plates. Stronger orientational polarization after doping, attributed to the increase of the amount of oxygen vacancies and zinc interstitials in ZnO nanostructures, led to an increase of dipole momentum and, in turn, to orientational polarization. AC conductivity of the prepared samples was found to increase with increase in frequency and complex impedance analysis showed single circular arc type behavior, suggesting the dominance of grain boundary resistance in all the samples.

Acknowledgments

The author Reza Zamiri and Budhendra Singh would like to express their personal thanks to FCT (Fundaçãopara a Ciência e a Tecnologia) for post-doctoral research Grants with reference numbers (SFRH/BPD/76185/2011) and SFRH/BPD/76184/2011, respectively.

References

[1] X. Du, Y. Fu, S. Tan, J. Luo, A. Flewitt, S. Maeng, S. Kim, Y. Choi, D. Lee, N. Park, ZnO film for application in surface acoustic wave device, Journal of Physics: Conference Series 76 (2007) 012035 (IOP Publishing).

[2] Y.-H. Ni, X.-W. Wei, J.-M. Hong, Y. Ye, Hydrothermal preparation and optical properties of ZnO nanorods, Materials Science and Engineering B 121 (1) (2005) 42–47.

[3] R. Viswanath, S. Ramasamy, R. Ramamoorthy, P. Jayavel, T. Nagarajan, Preparation and characterization of nanocrystalline ZnO based materials for varistor applications, Nanostructured Materials 6 (5) (1995) 993–996.

[4] J.-H. Lee, K.-H. Ko, B.-O. Park, Electrical and optical properties of ZnO transparent conducting films by the sol–gel method, Journal of Crystal Growth 247 (1) (2003) 119–125.

[5] R. Zamiri, A. Zakaria, H.A. Ahangar, M. Darroudi, A.K. Zak, G.P. Drummen, Aqueous starch as a stabilizer in zinc oxide nanoparticle synthesis via laser ablation, Journal of Alloys and Compounds 516 (2012) 41–48.

[6] R. Zamiri, A. Kaushal, A. Rebelo, J. Ferreira, Er doped ZnO nanoplates: synthesis, optical and dielectric properties, Ceramics International, in press.

[7] R. Zamiri, A. Lemos, A. Reblo, H.A. Ahangar, J. Ferreira, Effects of rare-earth (Er, La and Yb) doping on morphology and structure properties of ZnO nanostructures prepared by wet chemical method, Ceramics International, in press.

[8] J. She, Z. Xiao, Y. Yang, S. Deng, J. Chen, G. Yang, N. Xu, Correlation between resistance and field emission performance of individual ZnO one-dimensional nanostructures, ACS Nano 2 (10) (2008) 2015–2022.

[9] S. Baruah, J. Dutta, Hydrothermal growth of ZnO nanostructures, Science and Technology of Advanced Materials 10 (1) (2009) 013001.

[10] M. Soosen Samuel, J. Koshy, A. Chandran, K. George, Optical phonon confinement in ZnO nanorods and nanotubes, Indian Journal of Pure and Applied Physics 48 (2010) 703–708.

[11] K. Elen, H. Van den Rul, A. Hardy, M.K. Van Bael, J. D'Haen, R. Peeters, D. Franco, J. Mullens, Hydrothermal synthesis of ZnO nanorods: a statistical determination of the significant parameters in view of reducing the diameter, Nanotechnology 20 (5) (2009) 055608.

[12] H. Yan, J. Hou, Z. Fu, B. Yang, P. Yang, K. Liu, M. Wen, Y. Chen, S. Fu, F. Li, Growth and photocatalytic properties of one-dimensional ZnO nanostructures prepared by thermal evaporation, Materials Research Bulletin 44 (10) (2009) 1954–1958.

[13] P. Sahay, S. Tewari, R. Nath, S. Jha, M. Shamsuddin, Studies on ac response of zinc oxide pellets, Journal of Materials Science 43 (13) (2008) 4534–4540.

[14] J. Jose, M. Abdul Khadar, Role of grain boundaries on the electrical conductivity of nanophase zinc oxide, Materials Science and Engineering A 304 (2001) 810–813.

[15] L. Pinckney, Transparent glass-ceramics based on ZnO crystals, Physics and Chemistry of Glasses – European Journal of Glass Science and Technology Part B 47 (2) (2006) 127–130.

[16] S.A. Ansari, A. Nisar, B. Fatma, W. Khan, A. Naqvi, Investigation on structural, optical and dielectric properties of Co doped ZnO nanoparticles synthesized by gel-combustion route, Materials Science and Engineering B 177 (5) (2012) 428–435.

[17] J. Fan, R. Freer, The roles played by Ag and Al dopants in controlling the electrical properties of ZnO varistors, Journal of Applied Physics 77 (9) (1995) 4795–4800.

[18] C. Youn, T. Jeong, M. Han, J. Kim, Optical properties of Zn-terminated ZnO bulk, Journal of Crystal Growth 261 (4) (2004) 526–532.

[19] B. Jusserand, M. Cardona, M. Cardona, G. Güntherodt, Light scattering in solids V, Topics in Applied Physics 66 (1989) 49.

[20] N. Hasuike, R. Deguchi, H. Katoh, K. Kisoda, K. Nishio, T. Isshiki, H. Harima, Structural properties of nanometre-sized ZnO crystals doped with Co, Journal of Physics: Condensed Matter 19 (36) (2007) 365223.

[21] C. Koops, On the dispersion of resistivity and dielectric constant of some semiconductors at audiofrequencies, Physical Review 83 (1) (1951) 121.

[22] K.W. Wagner, Zur theorie der unvollkommenen dielektrika, Annalen der Physik 345 (5) (1913) 817–855.

[23] M.B. Reddy, P.V. Reddy, Low-frequency dielectric behaviour of mixed Li–Ti ferrites, Journal of Physics D: Applied Physics 24 (6) (1991) 975.

[24] S. Watawe, B. Sarwade, S. Bellad, B. Sutar, B. Chougule, Microstructure, frequency and temperature-dependent dielectric properties of cobalt-substituted lithium ferrites, Journal of Magnetism and Magnetic Materials 214 (1) (2000) 55–60.

[25] X.B. Wang, C. Song, K.W. Geng, F. Zeng, F. Pan, Luminescence and Raman scattering properties of Ag-doped ZnO films, Journal of Physics D: Applied Phyics 39 (2006) 4992.

[26] A. Maddalena, R. Dal Maschio, S. Dire, A. Raccanelli, Electrical conductivity of tin oxide films prepared by the sol–gel method, Journal of Non-Crystalline Solids 121 (1) (1990) 365–369.

[27] C. Li, J. Wang, W. Su, H. Chen, W. Zhong, P. Zhang, Effect of Mn^{2+} on the electrical nonlinearity of (Ni, Nb)-doped SnO_2 varistors, Ceramics International 27 (6) (2001) 655–659.

[28] R. Parra, J. Varela, C. Aldao, M. Castro, Electrical and microstructural properties of (Zn, Nb, Fe)-doped SnO_2 varistor systems, Ceramics International 31 (5) (2005) 737–742.

[29] A. Molak, M. Paluch, S. Pawlus, J. Klimontko, Z. Ujma, I. Gruszka, Electric modulus approach to the analysis of electric relaxation in highly conducting $(Na_{0.75}Bi_{0.25})(Mn_{0.25}Nb_{0.75})O_3$ ceramics, Journal of Physics D: Applied Physics 38 (9) (2005) 1450.